Meteorology and Climatology of Historical Weekly Wind and Solar Power Resource Droughts over western North America in ERA5

Patrick T Brown (patrick.brown@sjsu.edu)
San Jose State University https://orcid.org/0000-0002-5058-1718
David J. Farnham
Carnegie Institution Department of Global Ecology
Ken Caldeira
Carnegie Institution Department of Global Ecology

Research Article

Keywords: meteorology, climatology, wind energy, solar energy

Posted Date: April 19th, 2021

DOI: https://doi.org/10.21203/rs.3.rs-433450/v1

Meteorology and Climatology of Historical Weekly Wind and Solar Power Resource Droughts over western North America in ERA5

Patrick T. Brown[1*], David J. Farnham[2], Ken Caldeira[2]

[1] *Department of Meteorology and Climate Science, San José State University, San José, California, USA*

[2] *Department of Global Ecology, Carnegie Institution for Science, Stanford, California, USA*

Submitted to: *Climate Dynamics*

*Corresponding author: Patrick T. Brown, patrick.brown@sjsu.edu

Abstract

Wind and solar electricity generation is projected to expand substantially over the next several decades due both to rapid cost declines as well as regulation designed to achieve climate targets. With increasing reliance on wind and solar generation, future energy systems may be vulnerable to previously underappreciated synoptic-scale variations characterized by low wind and/or surface solar radiation. Here we use western North America as a case study region to investigate the historical meteorology of weekly-scale "droughts" in potential wind power, potential solar power and their compound occurrence. We also investigate the covariability between wind and solar droughts with potential stresses on energy demand due to temperature deviations away human comfort levels. We find that wind power drought weeks tend to occur in late summer and are characterized by a mid-level atmospheric ridge centered over British Columbia and high sea level pressure on the lee side of the Rockies. Solar power drought weeks tend to occur near winter solstice when the seasonal minimum in incoming solar radiation co-occurs with the tendency for mid-level troughs and low pressure systems over the U.S. southwest. Compound wind and solar power drought weeks consist of the aforementioned synoptic pattern associated with wind droughts occurring near winter solstice when the solar resource is at its seasonal minimum. We find that wind drought weeks are associated with high solar power (and vice versa) both seasonally and in terms of synoptic meteorology, which supports the notion that wind and solar power generation can play complementary roles in a diversified energy portfolio at synoptic spatiotemporal scales over Western North America.

Background

Energy System Transition. Global energy consumption by human activities relies largely on fossil fuels that cause global warming and reduce air quality (Oppenheimer and Petsonk, 2005). Thus, governments throughout the world have pursued agreements to decarbonize their economies by implementing policies that encourage an accelerated transition away from fossil fuels (UNFCCC, 2015).

Proposals to decarbonize economies often call for a higher share of total energy consumption to originate from electricity and for that electricity to be generated by non-greenhouse gas emitting technologies (Rogelj et al., 2018). These technologies include wind, solar, nuclear, hydroelectric, and geothermal power, among others. In 2018, wind and solar power accounted for only ~3% of total global energy consumption (BP Statistical Review of World Energy, 2020). However, over the 2010s, the cost of utility-scale wind and solar power declined by 70% and 90% respectively (Lazard, 2020) and in an optimistic scenario, the United States Energy Information Administration projects the cost of wind power to decline by a further 60% and the cost of solar power to decline by a further 75% by 2050 (US EIA, 2020).

These considerations suggest that the global energy infrastructure may be in the early stages of a transition away from electricity generated from mostly fossil fuels and towards electricity generation from near-zero greenhouse gas emissions energy sources, with a substantial fraction generated from wind and solar power. Projections and proposals vary widely, but some call for over 90% of United States electricity to be generated via wind turbines and solar collectors by the 2030s to 2050s

Congressional Action Plan, 2020; Jacobson et al., 2017; Larson et al., 2020; Williams et al., 2014). Regardless of their penetration levels by mid-century, wind and solar power should continue to expand in the near-term because, at their current fractional penetration levels, wind and solar power are cost-competitive or cheaper than fossil fuels on a levelized cost of energy (LCOE) basis. However, the total system costs of incorporating wind and solar power scale exponentially as a larger fraction is added to the grid due to their variability (Sepulveda et al., 2018; Shaner et al., 2018).

Challenges associated with wind and solar variability. Electricity demanded by society must be continuously matched by electricity supplied and thus the primary drawback to wind and solar power is that the resource fueling this electricity is intrinsically variable and does not vary in accordance with demand for energy (Gowrisankaran et al., 2016; Trainer, 2012; Ueckerdt et al., 2013).

Energy storage is expected to be capable of redistributing solar power collected during the day to the nighttime hours (Albertus et al., 2020), however, storage costs would need to come down roughly two orders of magnitude in order to allow for near 100% renewable electricity systems to cope with longer term variability in the wind and solar resource, while keeping system costs near their current levels (Sepulveda et al., 2018; Tong et al., 2020).

Additionally, correlation within a resource across space or correlation between wind and solar resources, represents a challenge to robust, continuous generation of electricity because a reduction in one resource would imply a simultaneous reduction in others (Shaner et al., 2018). Thus, the ability to transmit electricity over large

geographic areas is advantageous not only because it is most economically efficient to site wind and solar farms at relatively remote locations where it is climatologically windiest and sunniest, but also because pooling resources over large areas reduces the correlation between and within resources, making the total energy supply less variable (Jurasz et al., 2020; Jurasz et al., 2021; Rinaldi et al., 2021; Solomon et al., 2020; Weschenfelder et al., 2020; Yan et al., 2020).

Purpose of Article. Even renewable energy systems that incorporate long-distance transmission and sufficient energy storage to buffer the daily solar cycle will still be vulnerable to synoptic-scale weather events (i.e. at the several thousand kilometer spatial scale and several day timescale) characterized by particularly low wind resources, low surface solar radiation and/or large heating or cooling demands. The purpose of this article is to document the meteorology behind historical synoptic-scale reductions in potential wind and solar power energy resources (i.e., "droughts" (Rife, 2016)) as well as their associations with temperature deviations away from human comfort levels that could stimulate electricity demand.

This study is particularly focused on the historical *meteorology and climatology* of such events (as opposed to their impact on historical or hypothetical energy systems). Thus, we investigate variables averaged over a large domain without regard to particularities of the spatial distribution of wind farms, solar farms or population. This allows us to study the physical relationships between the meteorological variables as a foundation for future work that can address questions specific to particular energy systems.

Details of Analysis

When designing the analysis, we were conscious that there is a trade-off between practical usefulness and the illumination of fundamental physical understanding. In this study we strongly emphasize the latter and we do not deal with any practical sociological, technological, or political constraints. Thus, in this study, we take a plot of land roughly the size of an existing electricity grid and document how potential wind power, potential solar power, and temperature deviations away from 65 degrees (i.e., pseudo heating and cooling degree days experienced by land not people) vary and covary at weekly timescales.

Spatiotemporal scale of analysis. In this work we study the weekly timescale as it is relevant for the type of energy system that may exist within the next several decades where there is sufficient energy storage and transmission to adequately buffer the daily solar cycle but not necessarily longer-term variation in wind and solar energy supply (Albertus et al., 2020). The weekly timescale also encapsulates the societal cycle in electricity demand associated with the calendar week.

The spatial scale studied here was chosen to be roughly the size of existing large power grids (several million square kilometers). We study an area that approximately encompasses the existing Western Interconnection (WECC) power grid (Fig. 1). This region of western North America (WNA) contains substantial annual mean wind and solar power resources (Jacobson and Delucchi, 2011; MacDonald et al., 2016; Pryor and Barthelmie, 2011). These resources, however, are subject to substantial seasonal

111 and synoptic variability (Millstein et al., 2019; Rinaldi et al., 2021; Wang et al., 2018;
112 Wang et al., 2020).

113 From a meteorological perspective, the weekly timescale and several million square
114 kilometer spatial scale is relevant because these are the scales for which Rossby
115 Waves often manifest at mid latitudes. Rossby Waves would typically traverse our
116 WNA domain in ½ to 2 ½ days so an individual trough or ridge would typically be a
117 transient phenomenon at the weekly timescale. Nevertheless, the coincidence of two
118 or three such waves of similar character within a week, or a slow-moving cut-off low
119 or blocking high, would cause persistent weather conditions over the domain at the
120 weekly timescale.

121 This is also a natural spatiotemporal scale to study as it has a long meteorological
122 history in the explanation of temperature and precipitation variability. Such
123 variability is often discussed in the context of preferred states of the atmosphere
124 quantified with teleconnection indices like the Pacific North American Pattern (PNA)
125 (Wallace and Gutzler, 1981), Arctic Oscillation (AO) (Thompson and Wallace, 1998),
126 and the North Atlantic Oscillation (NAO) (Hurrell, 1995), among others. For example,
127 the NOAA Synoptic Discussion typically averages variables over the one week
128 timescale in their retrospective reports on U.S. weather and often discusses these
129 events in the context of the above teleconnection indices (NOAA, 2021).

130 Finally, extreme weather at this spatiotemporal scale has had a demonstrable impact
131 on electricity grids historically. For example, the rotating electricity outages
132 implemented by the California Independent System Operator Corporation (CAISO) in

mid-August 2020 were associated with a thermal ridge over the western half of the United States that corresponded to a strongly positive PNA pattern evident from August 15-21 (NOAA, 2020). Another pertinent example was the extreme cold event experienced in mid-February 2021 that led to widespread electricity outages in Texas (IEA, 2021). That event was associated with a persistent trough over the central United States, which corresponds to a strongly negative AO (NOAA, 2021).

The above two instances of electric grid failure were caused mostly by sharp increases in electricity demand for cooling and heating, but both were exacerbated by some reduction in renewable resources and they serve to highlight a spatiotemporal scale at which electricity systems are sensitive. Here we focus on extreme reductions in the wind and solar power resources at roughly the same spatiotemporal scales.

Wind and Solar droughts.

Henceforth in this study, we refer to a "drought" as a week in which the wind power resource or the solar power resource (or their combination), averaged over the entire week and the entire domain (Fig. 1), is in the first percentile of all weeks considered (from 1950-2020). A first percentile week corresponds to a return period of approximately two years. The first percentile is defined with respect to the entire record, not with respect to the mean for that calendar week of the year. We define droughts this way because, from an energy system perspective, the absolute magnitude of the energy resource is what is relevant for meeting electricity demand, not the anomaly relative to the typical seasonal cycle. This is different than the consideration for hydrological droughts in which human and natural systems are

thought to already be accustomed and/or adapted to the seasonal cycle and thus it is deviations away from this seasonal cycle that are most important.

The spatial component of the definition of a drought is arbitrary but in this paper we define droughts as lulls in the resource averaged over the entire domain which is roughly the size of the Western Interconnection electricity grid where wind and solar resources might be able to be pooled (Fig. 1).

For compound wind and solar droughts we find the first percentile weeks after both resources have been normalized by their mean over the entire record and summed,

$$"compound\ wind\ and\ solar\ droughts" = 1^{st} percentile\left[\frac{wind\ power(t)}{mean(wind\ power(t))} + \frac{solar\ power(t)}{mean(solar\ power(t))}\right].$$

In order to illustrate the characteristic atmospheric circulation configuration associated with wind droughts, solar droughts and compound wind and solar droughts we show composites of many variables over all drought weeks in the dataset (Figs 3, 4 and 5). The length of our dataset is 71 years (1950-2020 inclusive) which is 3,692 weeks. Thus, there are 37 weeks that make up the first percentile. To measure coherence between drought events we stipple the locations where at least 75% (28 out of 37) of the drought weeks agree in the sign of their anomaly (with respect to that calendar week of the year).

Variables and Data. All of our analysis is conducted using ERA5 reanalysis data from 1950-2020 (Hersbach et al., 2020). ERA5 assimilates a large amount of observations into a dynamical weather model to produce a physically-consistent estimation of the state of the ocean, atmosphere and land surface. We use 1°×1° output within the WNA

domain (Fig. 1), and 2.5°×2.5° for the Northern Hemisphere atmosphere outside of the domain (Figs 4-5).

Since we are interested in the wind's capacity to be converted into electricity, we convert hourly wind speed values at 100 meters altitude to hourly wind power at 100 meters via the power curve shown in Fig. S1 based on the wind turbine power curve from a V90-2.0MW Vestas turbine. We then convert the power generated by each turbine to power per unit area (i.e. W/m^2) by assuming a required land area per turbine equal to four times the rotor diameter in one direction and seven times the rotor diameter in the other direction (Lu and McElroy, 2017). Since the rotor diameter of the 2 MW wind turbine is 90 m, we assume that each turbine takes up about ~0.23 km^2 of land area. The hourly wind power was then averaged to the weekly scale prior to drought analysis.

For the solar resource, we used hourly downward incident surface solar radiation which was also averaged to the weekly scale prior to drought analysis. We do not convert these values into the effective extractible solar power because conversion would require making assumptions about extraction technology and/or the tilt and tracking capability of hypothetical solar arrays. While our use of the raw downward incident surface solar radiation is reasonable for our analysis that focuses on *normalized* variability of the resource (i.e. variability of the resource with respect to its own mean), it does mean that the values in Fig. 1d-f are much larger than could be practically extracted from solar farms in those locations

ERA5 atmospheric data has a resolution of 31km (T639). This resolution is not sufficient to represent mesoscale and boundary layer features that will impact short-timescale variability at the level of particular wind/solar farms. Nevertheless, previous studies have indicated that ERA5 is sufficient to conduct renewable energy analysis at the courser resolution that we consider here (Jurasz et al., 2021; Olauson, 2018; Ramirez and Schmidt, 2020). Additionally, we compare our ERA5-derived variables over specific regions where wind and solar generation data was available from the US Energy Information Administration to confirm that the variability of our reanalysis-inferred solar and wind resources is a reasonable representation of the variability of measured generation in those locations (Figs S2 and S3).

We also considered daily mean temperature ($[T_{min} + T_{max}]/2$) departures from 65°f (18°C) where positive departures represent cooling degree days (CDDs) and negative departures represent heating degree days (HDDs). We investigate these quantities because they represent the geophysical variables most likely to affect demand-side stress on the energy system (Mourshed, 2016; Petri and Caldeira, 2015). However, because we want to focus on the physical relationships between wind, surface solar radiation and temperature, regardless of the particularities of the energy system/population distribution, we do not weigh these CDDs or HDDs by population. Thus, in this paper we discuss CDDs and HDDs experienced by land, not people.

As mentioned above, all values were averaged to the weekly scale prior to subsequent analysis. In order to simplify the analysis and deal with leap years, the first week of each year was defined to begin on January 1st of that year and 52 weeks were included

219 in each year. This meant that the first 364 days of each year were included in our
220 analysis and the last one or two days of each year were not included.

221 **Results**

222 We first establish the contextual long-term climatology of wind power, solar power,
223 and heating/cooling degree days (experienced by land) prior to investigating their
224 most extreme weeks.

225 ***Spatial long-term climatology.*** Most of the wind power supply is located on the lee
226 side (i.e., to the east) of the Rocky Mountains in the U.S.'s "wind corridor" (Fig. 1a, 1b,
227 and 1c). There is little seasonal spatial shift in the location of the maximum wind
228 supply and instead the stationary pattern intensifies in winter and weakens in
229 summer (c.f. Fig. 1a and 1b).

230 The surface solar power resource is concentrated in the southwest corner of the
231 domain but is more homogeneous than the wind power resource because topography
232 exerts a smaller influence on cloud cover than it does on near surface atmospheric
233 flow. Near the summer solstice, the meridional gradient of top-of-atmosphere daily
234 mean incoming solar radiation is very small so most of the spatial variation in surface
235 solar radiation is due to cloud cover (Fig. 1e). Because of this, summer zonal gradients
236 in incident solar radiation can be as large as meridional gradients. Near the winter
237 solstice, on the contrary, the meridional gradient of incident daily mean incoming
238 solar radiation is dominant (Fig. 1d).

239 The seasonal cycle in HDDs and CDDs is as would be expected. Most of the domain
240 has a long-term daily mean temperature colder than 18°C so there are more HDDs

than CDDs (c.f. Fig 1l and Fig. 1i). Seasonally, this affect is most pronounced in the winter when there is nearly zero land experiencing CDDs (Fig. 1g) but substantial HDDs (over 30 HDDs per day over most of the higher latitudes and elevations; Fig. 1j). Even in the summer there are only slightly more CDDs than HDDs when averaged over the domain (c.f. Fig 1h and Fig. 1k). Despite this, because of the larger use of electricity for cooling than for heating and because of the tendency for people to live in wamer climates, electiricty demand over the Western Interconnection tedns to peak in the late summer(Rinaldi et al., 2021). This pattern of a dual peak in demand (one corresponding to the winter peak in HDDs and one corresponding to the summer peak in CDDs is observed in actual load data for the United States.

Seasonal long-term climatology. The right side of figure 1 shows the mean and standard deviation of the seasonal cycle for the solar power resource, the wind power resource, HDDs and CDDs averaged over the entire WNA domain. All values are expressed as a fraction of their long-term mean value.

The solar power resource runs from ~40% of its annual mean near the winter solstice to ~160% of its annual mean near the summer solstice (Fig. 1m). Variability in solar power is dominated by the seasonal cycle. This suggests that solar droughts (as defined here using absolute minimum weeks over the entire period) will occur during the weeks near the winter solstice (squares in Fig. 1m and 1n).

The seasonal cycle in wind power is slightly anticorrelated with the seasonal cycle in solar power but its phase lags that of solar power by about five weeks (Fig. 1m). The amplitude of the seasonal cycle in wind power is much less than the amplitude of the

seasonal cycle in solar power. Wind power supply is about 110% above its annual mean for much of the cooler portion of the year and it dips to about 60% of its annual mean in mid to late summer when the Northern Hemisphere meridional temperature gradient, and thus upper-level geostrophic wind, is at an annual minimum. However, wind power variability is dominated by synoptic weather conditions rather than the seasonal cycle. This implies that a wind drought can plausibly occur at any time of the year but that they are most-likely in the late summer in July and August (Fig. 1m).

Overall, weekly solar power has 167% of the variability of weekly wind power and weekly solar variability is dominated by the seasonal cycle (99% of weekly solar variability is linearly explained by the week-of-the-year) while wind power variability is dictated more by atmospheric circulation variability (only 42% of weekly wind variability is linearly explained by the week-of-the-year).

Weekly wind and solar values. Figure 2 shows the domain mean for each week in the dataset plotted in a two-dimensional wind power and solar power space with CDDs displayed as colors (Fig. S4 shows the corresponding figure with HDDs). Wind droughts are shown as circles with black outlines, solar droughts as squares with black outlines and compound wind and solar droughts as diamonds with black outlines (same as in Fig. 1m and 1n).

Wind droughts tended to occur in astronomical summer (Fig. 1m and Quadrant II in Fig. 2). During wind droughts, solar power averaged ~139% of its long-term mean (large dark circle in figure 2), with a tendency towards increased CDDs and decreased HDDs.

Solar droughts all occurred around the winter solstice (Fig. 1m and Quadrant III and Quadrant IV in Fig. 2). During solar droughts, wind power had a mean of ~112% of its long-term mean (large dark square in Fig. 2), with a tendency towards decreased CDDs and increased HDDs.

Simultaneously considering the proxies for energy supply (Fig. 1m and axes of Fig. 2) and energy demand (Fig. 1n and colors of Fig. 2 and Fig. S4), the least stress on the energy system would be experienced in the astronomical spring when both wind and solar power tend to be above their long-term mean and both HDDs and CDDs are near their long-term mean. Conversely, the most stress on the energy system tends to occur in the astronomical autumn (Quadrant III of Fig. 2), when there tends to be low solar power and still the substantial possibility for low wind power. HDDs are also high at this time (Fig. S4), potentially adding stress on the demand side of an underlying energy system if that system uses electricity for heating.

There are 20 weeks in the 71 year time period where CDDs were above their long term mean while both wind and solar resources were below their long term mean (pink and red circles in Quadrant III of Fig. 2). None of these weeks reach the wind/solar drought threshold so we will not focus on them here but they nevertheless indicate potentially large stress on an underlying energy system and may merit study in future research.

Compound wind and solar droughts all occur near the winter solstice (Fig. 1m and Quadrant III in Fig. 2). This is because the dominance of the seasonal cycle in solar power confines the compound wind and solar droughts to this time of the year.

During compound wind and solar droughts, solar power tends to be ~41% of its annual mean and wind power tends to be ~70% of its annual mean (dark diamond in Fig. 2), with a tendency towards decreased CDDs and increased HDDs (Fig. S4). Thus heating demand is more of a concern than cooling demand with regard to electricity demand increases exacerbating compound wind and solar droughts.

Synoptic meteorology of wind and solar droughts. Here we assess the first-order, proximate, synoptic-dynamic mechanisms associated with wind and solar droughts. From this perspective, our expectation is that surface high pressure systems will be associated with subsidence, clear skies (enhanced surface solar radiation) and calm conditions. On the other hand, surface low pressure systems will be associated with ascent, clouds (reduced surface solar radiation) and enhanced wind.

We connect surface high and low pressure systems to dynamic "forcing" aloft by invoking Quasi-Geostrophic (QG) Theory (Carlson, 1994; Charney, 1948). QG theory states that under a number of assumptions that are plausible at synoptic spatiotemporal scales, vertical motion in the atmosphere is related to non-geostrophic circulations that restore thermal wind balance: Positive (negative) differential vorticity advection by the geostrophic wind is associated with divergence (convergence) aloft, ascent (subsidence) and low (high) surface pressure. Also, relatively warm (cold) temperature advection by the geostrophic wind implies upward (downward) vertical motion over the lower half of the atmosphere which is associated with surface low (high) pressure. We use a standard meteorological convention of investigating vorticity advection via the relative vorticity at 500mb

(Fig. 5d. 5e. and 5f.) and temperature advection at the 700mb level temperature (Fig. 5g. 5h. and 5i.).

Wind droughts. Figure 3 shows the average spatial anomalies of wind power, solar power, and temperature variables during drought events. During a typical wind drought, the entire WNA domain tends to experience reduced wind with respect to the mean for that week of the year (spatial average of 43% of typical wind power, Fig. 3a). During a wind drought, solar power tends to be both above-average seasonally (139% long-term mean) and slightly above average with respect to the mean for that week of the year (102%, Fig. 3d). Thus, wind droughts tend to be accompanied by slightly enhanced solar availability. However, wind droughts are consistently associated with slightly less solar power than average over the climatologically sunniest region (indicated by the stippling on the bottom half of the WNA domain in Fig. 3d).

During wind droughts, it tends to be warmer than average to the north where climatological temperatures are below 18°C and colder than average to the south where climatological temperatures are above 18°C (Fig. 3g). This is indicative of a simultaneous reduction in HDDs *and* CDDs potentially reducing stress on the demand side of a hypothetical underlying energy system.

Wind droughts tend to be associated with a warm core (dynamic) high over British Columbia flanked by cold core lows on either side (Fig. 4d and 5g). This is reminiscent of a positive Pacific North American (PNA) Pattern that accentuates the typical

meridional deviations in the large-scale atmospheric flow, making it wavier than normal and possibly generating more persistent conditions.

At mid-levels, we see convergence over most of the WNA domain (Fig. 5a) associated with subsidence and high sea level pressure (Fig. 4g). One reason for this is likely the negative vorticity advection on the downstream side of ridge (Fig. 5d) and the negative vorticity advection associated with the left entrance region of a jet streak at 250mb (Fig. 4a). Additionally, cold air advection over some of the eastern side of the domain also promotes subsidence (Fig. 5g). Some positive vorticity advection and divergence is also observed near the southwest U.S. (Fig. 5a and 5d) which would typically be associated with upward vertical motion and thus is consistent with the region experiencing anomalously cloudy conditions (Fig. 3d).

Sea surface temperature anomalies show a pattern reminiscent of a western Pacific El Niño occurring during an enhanced Aleutian low (Alexander et al., 2002) and a positive phase of the Pacific Decadal Oscillation (PDO, (Brown et al., 2014; Brown et al., 2017; Power et al., 1999)) (Fig. 4j). However, the lack of widespread stippling indicates that this is not a necessary condition for a wind drought and that they can easily occur under a diverse set of sea surface temperature patterns (Fig. S12).

Solar droughts. During a typical solar drought, almost the entire WNA domain consistently experiences reduced solar power with respect to the week-of-the-year (spatial average of 94% of typical values, Fig. 3e). Also, during a solar drought, there tends to be more wind power than average overall (112% long-term mean, Fig. 3b) and it tends to be windier than average with respect to the mean for that week of the

year (103%, Fig. 3b). This is further evidence of an inverse relationship between wind and solar power. This anomalously high wind power is centered over the southwest U.S. but a lack of stippling indicates that the spatial manifestation of this feature is not consistent across solar drought events (see Fig. S6).

During a typical solar drought, the surface over most of the domain tends to be warmer than average for that week of the year (Fig. 3h). Since the entire domain is typically below 18°C during the winter (Fig. 1j), this reduces HDDs. Thus, the stress-inducing impact of solar droughts on a hypothetical underlying energy system may be partially mitigated by their co-occurrence with reduced HDDs.

Solar droughts tend to be associated with cold core (dynamic) lows occurring on the west coast of the U.S. (Fig. 4e and 4h). This damps the typical meridional deviations in the large-scale flow, making it more zonal than normal and possibly contributes to the relative lack of persistence of solar droughts compared to wind droughts.

At mid-levels, we see divergence off the west coast of WNA (Fig. 5b), which in turn is associated with ascent, low sea level pressure (Fig. 4h), high winds (Fig. 3b) and cloudier than normal conditions (Fig. 3e). One reason for this is likely the positive shear vorticity advection off the west coast of WNA (Fig. 5e) and the positive vorticity advection associated with the left exit region of a jet streak on the northwest side of the WNA domain at 250mb (Fig. 4b). Additionally, some slight warm air advection is seen off the west coast of WNA which also is associated with ascent (Fig. 5h).

We see some evidence that solar droughts are associated with the positive state of the North Atlantic Oscillation ((Deser et al., 2010; Hurrell, 2003) Fig. 4h and 4k), and

are slightly associated with the negative phase of Atlantic Multidecadal Variability ((Schlesinger and Ramankutty, 1994) AMV, Fig. 4k) but with little consistency across events (see the diversity of patterns in Fig. S13).

Compound wind and solar droughts. Compound wind and solar drought events tend to be similar in character to wind drought events in terms of their surface manifestation (c.f. the right and left columns of Fig. 3), and their circulations (c.f. the right and left columns of Figs 3 and 4). There is relatively little atmospheric circulation influence on surface solar radiation (relative to the influence of the seasonal cycle) and thus it is the atmospheric influence on the wind that dictates the occurrence of compound wind and solar droughts.

During the typical compound wind and solar drought, it tends to be colder than average over most of the domain (Fig. 3i). This increases the HDDs since virtually the entire domain is climatologically below 18°C in the winter (Fig. 1g and 1j). This means that the stress of compound wind and solar droughts on a hypothetical underlying energy system could be exacerbated by their co-occurrence with increased HDDs.

Compound wind and solar drought events tend to be characterized by warm air advection (Fig. 5i), which would typically be associated with ascent, enhanced winds and storms. However, the negative vorticity advection (Fig. 5f) appears to cancel this effect, resulting in convergence aloft over the climatological windiest region (Fig. 5c).

Summary and discussion

The purpose of this article was to document the typical conditions and synoptic meteorology associated with extreme reductions in wind and solar energy resource

availability at the weekly timescale over Western North America (i.e., wind and solar "droughts").

We found that on the spatiotemporal scale selected (averaged weekly and over all of western North America), solar power varies 2/3^{rds} more (i.e., 167%) than wind power and that solar variability is dominated by the seasonal cycle (99% of weekly-mean solar variability is explained linearly by the week-of-the-year) while wind power variability is dictated more by atmospheric circulation variability (only 42% of weekly-mean wind variability is explained linearly by the week-of-the-year).

We found that wind droughts tend to occur in late summer when solar power is high, cooling degree days experienced by land tend to be high and heating degree days experienced by land tend to be low. Wind droughts are associated with surpluses in solar resources both due to the seasonal cycle and the synoptic weather setup. This supports the notion of added value for energy resource portfolios that include both wind and solar energy (Rinaldi et al., 2021).

Wind drought events were associated with a thermal mid-level ridge (warm core high) centered over British Columbia near the left entrance region of jet streak. This pattern was also accompanied by mid-level convergence, synoptic scale subsidence and surface high pressure due to negative vorticity advection and cold air advection into the region. This was associated with clear skies and sunnier/warmer conditions to the north. We found evidence that wind droughts were weakly associated with Western Pacific El Niño events during positive PDO but that they appear to emerge

predominantly from internal atmospheric variability rather than requiring sea surface temperature anomaly forcing.

We found that solar drought events were confined to near the winter solstice when available wind power tends to be high, CDDs tend to be low and HDDs tend to be high. Solar drought events were associated with a thermal mid-level trough (cold core low) off of the west coast of North America near the left exit region of a jet streak. This pattern was also accompanied by mid-level divergence and synoptic scale ascent due to positive vorticity advection and warm air advection into the region. This was associated with surface low pressure, cloudy, windy and warm conditions in the southwest U.S. There is some evidence that this is associated with a positive North Atlantic Oscillation-like signature, which suggests some potential predictability (Smith et al., 2020).

We found that compound wind and solar droughts resulted from atmospheric circulation patterns reminiscent of wind droughts but that they occurred in the winter when there was little available solar power. Compound wind and solar droughts occurred seasonally when HDDs were largest and the synoptic circulation associated with the compound drought events exacerbates this to a small degree. This means that the electrification of heating could potentially make these compound wind and solar droughts high stress events on a hypothetical underlying energy system (though this may be simultaneously mitigated by global warming).

The synoptic-dynamic meteorology of the wind and solar droughts studied here conformed to the first-order expectations informed by Quasi-Geostrophic Theory.

This indicates that these droughts are manifestations of well-known weather patterns and are not the result of some unexpected or exotic mechanism. This is evidence that wind and solar droughts should be as forecastable as any synoptic weather phenomena on daily to seasonal timescales and it suggests that they should be represented reasonably well by courser resolution climate models.

The dipole-like wave patterns in Fig. 4d, 4e and 4f suggest opposite anomalies on the eastern and western sides of North America meaning that below normal wind power (above normal solar power) on the western side of North America would be compensated for by above normal wind power (below normal solar power) on the eastern side of North America. This supports the notion that there is value in moving towards a continental scale "supergrid" connected by high voltage transmission (Larson and Swan, 2020). This may be the case more generally in the sense that electric grids at midlatitudes could greatly benefit from being large enough to encompass the full wavelength of typical Rossby Waves.

Looking forward, mean changes in the wind and solar resource are possible over WNA that could shift the likelihood of wind and solar drought events. Long-term mean incident surface solar radiation is expected to remain roughly steady (Feron et al., 2021) or perhaps increase slightly (Gernaat et al., 2021) due to decreases in relative humidity and clouds over land (Collins et al., 2013) while long-term mean wind change is uncertain (Pryor and Barthelmie, 2011) with some studies suggesting a slight increase (Gernaat et al., 2021) and others suggesting a slight decrease (Karnauskas et al., 2018). We also expect progressively more cooling degree days and less heating degree days (Li et al., 2012). However, these trends in the long-term-

mean would not necessarily translate into proportional changes in the statistics of drought events which could be overwhelmed by the particulars of changes in atmospheric circulation like the frequency of atmospheric blocking events (Woollings et al., 2018). Nevertheless, we found very little evidence for robust changes in wind and solar droughts historically (not shown).

Overall, this documentary study serves as a prototype for future work that can focus on different locations, different spatiotemporal scales, changes over time, and/or can add more energy system specificity. Ultimately we hope that this may help provide a foundation for the scientific understanding of weather events that will be consequential for renewable energy systems of the future.

Declarations

Funding: This work was supported by a gift to Carnegie Institution for Science from Gates Ventures LLC and by proceeds of the Carnegie Institution endowment.

Conflicts of interest/Competing interests: None.

Availability of data and material: The ERA5 data used in this study can be downloaded at https://cds.climate.copernicus.eu/#!/search?text=ERA5&type=dataset.

Code availability: The code used for this analysis is archived at https://github.com/ptbrown31/wind_solar_drought.

References

2035 The Report. Goldman School of Public Policy, 2020. https://www.2035report.com/electricity/

NOAA National Centers for Environmental Information, State of the Climate: Synoptic Discussion for August 2020. 2020. https://www.ncdc.noaa.gov/sotc/synoptic/202008

NOAA National Centers for Environmental Information, State of the Climate: Synoptic Discussion for february 2021. https://www.ncdc.noaa.gov/sotc/synoptic/202101

US EIA, 2021. Annual Energy Outlook. https://www.eia.gov/outlooks/aeo/

Albertus, P., et al., 2020. Long-Duration Electricity Storage Applications, Economics, and Technologies. Joule. 4**,** 21-32.

Alexander, M. A., et al., 2002. The Atmospheric Bridge: The Influence of ENSO Teleconnections on Air–Sea Interaction over the Global Oceans. Journal of Climate. 15**,** 2205-2231.

BP Statistical Review of World Energy. 2020. https://www.bp.com/en/global/corporate/energy-economics/statistical-review-of-world-energy.html

Brown, P. T., et al., 2014. Regions of significant influence on unforced global mean surface air temperature variability in climate models. Journal of Geophysical Research: Atmospheres. 120**,** 480-494.

Brown, P. T., et al., 2017. Change in the magnitude and mechanisms of global temperature variability with warming. Nature Climate Change. 7**,** 743.

Carlson, T. N., 1994. Mid Latitude Weather Systems. American Meteorological Society.

Charney, J. G., 1948. On the Scale of Atmopsheric Motions. Geofysiske Publikasjoner. 17.

Collins, M., R. Knutti, J. Arblaster, J.-L. Dufresne, T. Fichefet, P. Friedlingstein, X. Gao, W.J. Gutowski, T. Johns, G. Krinner, M. Shongwe, C. Tebaldi, A.J. Weaver, M. Wehner, Long-term Climate Change: Projections, Commitments and Irreversibility. In: Climate Change 2013: The Physical Science Basis. Contribution of Working Group I to the Fifth Assessment Report of the Intergovernmental Panel on Climate Change [Stocker, T.F., D. Qin, G.-K. Plattner, M. Tignor, S.K. Allen, J. Boschung, A. Nauels, Y. Xia, V. Bex and P.M. Midgley (eds.)]. Cambridge, United Kingdom, 2013.

Solving the Climate Crisis, 2020. The Congressional Action Plan for a Clean Energy Economy and a Healthy Resilient and Just America. https://climatecrisis.house.gov/report

Deser, C., et al., 2010. Sea Surface Temperature Variability: Patterns and Mechanisms. Annual Review of Marine Science. 2**,** 115-143.

Feron, S., et al., 2021. Climate change extremes and photovoltaic power output. Nature Sustainability. 4, 270-276.

Gernaat, D. E. H. J., et al., 2021. Climate change impacts on renewable energy supply. Nature Climate Change. 11, 119-125.

Gowrisankaran, G., et al., 2016. Intermittency and the Value of Renewable Energy. Journal of Political Economy. 124, 1187-1234.

Hersbach, H., et al., 2020. The ERA5 global reanalysis. Quarterly Journal of the Royal Meteorological Society. 146, 1999-2049.

Hurrell, J. W., 1995. Decadal Trends in the North Atlantic Oscillation: Regional Temperatures and Precipitation. Science. 269, 676-679.

Hurrell, J. W. K., Y.; Ottersen G.; Visbeck M., 2003. The North Atlantic Oscillation: Climatic Significance and Environmental Impact. American Geophysical Union.

IEA, Severe power cuts in Texas highlight energy security risks related to extreme weather events. IEA, Paris, France, 2021.

Jacobson, M. Z., Delucchi, M. A., 2011. Providing all global energy with wind, water, and solar power, Part I: Technologies, energy resources, quantities and areas of infrastructure, and materials. Energy Policy. 39, 1154-1169.

Jacobson, M. Z., et al., 2017. 100% Clean and Renewable Wind, Water, and Sunlight All-Sector Energy Roadmaps for 139 Countries of the World. Joule. 1, 108-121.

Jurasz, J., et al., 2020. A review on the complementarity of renewable energy sources: Concept, metrics, application and future research directions. Solar Energy. 195, 703-724.

Jurasz, J., et al., 2021. Complementarity and 'Resource Droughts' of Solar and Wind Energy in Poland: An ERA5-Based Analysis. Energies. 14, 1118.

Karnauskas, K. B., et al., 2018. Southward shift of the global wind energy resource under high carbon dioxide emissions. Nature Geoscience. 11, 38-43.

Larson, E. et al., Net-Zero America: Potential Pathways, Infrastructure, and Impacts. interim report. Princeton University, Princeton, NJ, 2020.

Lazard, 2020. Levalized Cost of Energy Comparison.

Li, D. H. W., et al., 2012. Impact of climate change on energy use in the built environment in different climate zones – A review. Energy. 42, 103-112.

Lu, X., McElroy, M. B., Chapter 4 - Global Potential for Wind-Generated Electricity. In: T. M. Letcher, (Ed.), Wind Energy Engineering. Academic Press, 2017, pp. 51-73.

MacDonald, A. E., et al., 2016. Future cost-competitive electricity systems and their impact on US CO2 emissions. Nature Climate Change. 6, 526-531.

572 Millstein, D., et al., 2019. Wind energy variability and links to regional and synoptic scale
573 weather. Climate Dynamics. 52, 4891-4906.

574 Mourshed, M., 2016. Climatic parameters for building energy applications: A temporal-
575 geospatial assessment of temperature indicators. Renewable Energy. 94, 55-71.

576 Olauson, J., 2018. ERA5: The new champion of wind power modelling? Renewable Energy.
577 126, 322-331.

578 Oppenheimer, M., Petsonk, A., 2005. Article 2 of the UNFCCC: Historical Origins, Recent
579 Interpretations. Climatic Change. 73, 195-226.

580 Petri, Y., Caldeira, K., 2015. Impacts of global warming on residential heating and cooling
581 degree-days in the United States. Scientific Reports. 5, 12427.

582 Power, S., et al., 1999. Inter-decadal modulation of the impact of ENSO on Australia. Climate
583 Dynamics. 15, 319-324.

584 Pryor, S. C., Barthelmie, R. J., 2011. Assessing climate change impacts on the near-term
585 stability of the wind energy resource over the United States. Proceedings of the
586 National Academy of Sciences. 108, 8167-8171.

587 Ramirez Camargo, L., Schmidt, J., 2020. Simulation of multi-annual time series of solar
588 photovoltaic power: Is the ERA5-land reanalysis the next big step? Sustainable
589 Energy Technologies and Assessments. 42, 100829.

590 Rife, D. K., N.Y.; Cohan, D.S.; Collier, J.C., 2016. A new kind of drought: U.S. record low
591 windiness in 2015. Earthzine. https://earthzine.org/a-new-kind-of-drought-u-s-
592 record-low-windiness-in-2015/

593 Rinaldi, K. Z., et al., 2021. Wind and Solar Resource Droughts in California Highlight the
594 Benefits of Long-Term Storage and Integration with the Western Interconnect.
595 Environmental Science & Technology.

596 Rogelj, J., et al., 2018. Scenarios towards limiting global mean temperature increase below
597 1.5 °C. Nature Climate Change. 8, 325-332.

598 Schlesinger, M. E., Ramankutty, N., 1994. An oscillation in the global climate system of
599 period 65-70 years. Nature. 367, 723-726.

600 Sepulveda, N. A., et al., 2018. The Role of Firm Low-Carbon Electricity Resources in Deep
601 Decarbonization of Power Generation. Joule. 2, 2403-2420.

602 Shaner, M. R., et al., 2018. Geophysical constraints on the reliability of solar and wind power
603 in the United States. Energy & Environmental Science. 11, 914-925.

604 Smith, D. M., et al., 2020. North Atlantic climate far more predictable than models imply.
605 Nature. 583, 796-800.

606 Solomon, A., et al., Exploiting wind-solar resource complementarity to reduce energy
607 storage need. 2020.

608 Thompson, D. W. J., Wallace, J. M., 1998. The Arctic oscillation signature in the wintertime
609 geopotential height and temperature fields. Geophysical Research Letters. 25, 1297-
610 1300.

611 Tong, F., et al., 2020. Effects of Deep Reductions in Energy Storage Costs on Highly Reliable
612 Wind and Solar Electricity Systems. iScience. 23, 101484.

613 Trainer, T., 2012. A critique of Jacobson and Delucchi's proposals for a world renewable
614 energy supply. Energy Policy. 44, 476-481.

615 Ueckerdt, F., et al., 2013. System LCOE: What are the costs of variable renewables? Energy.
616 63, 61-75.

617 UNFCCC, UNFCCC Adoption of the Paris Agreement. I: Proposal by the President. 2015.

618 Wallace, J. M., Gutzler, D. S., 1981. Teleconnections in the Geopotential Height Field during
619 the Northern Hemisphere Winter. Monthly Weather Review. 109, 784-812.

620 Wang, M., et al., 2018. The future of wind energy in California: Future projections with the
621 Variable-Resolution CESM. Renewable Energy. 127, 242-257.

622 Wang, M., et al., 2020. Future projections of wind patterns in California with the variable-
623 resolution CESM: a clustering analysis approach. Climate Dynamics. 54, 2511-2531.

624 Weschenfelder, F., et al., 2020. A review on the complementarity between grid-connected
625 solar and wind power systems. Journal of Cleaner Production. 257, 120617.

626 Williams, J. H., B. Haley, F. Kahrl, J. Moore, A.D. Jones, M.S. Torn, H. McJeon, 2014. Pathways
627 to deep decarbonization in the United States. The U.S. report of the Deep
628 Decarbonization Pathways Project of the Sustainable Development Solutions
629 Network and the Institute for Sustainable Development and International Relations.

630 Woollings, T., et al., 2018. Blocking and its Response to Climate Change. Current Climate
631 Change Reports. 4, 287-300.

632 Yan, J., et al., 2020. Reviews on characteristic of renewables: Evaluating the variability and
633 complementarity. International Transactions on Electrical Energy Systems. 30,
634 e12281.

Figures

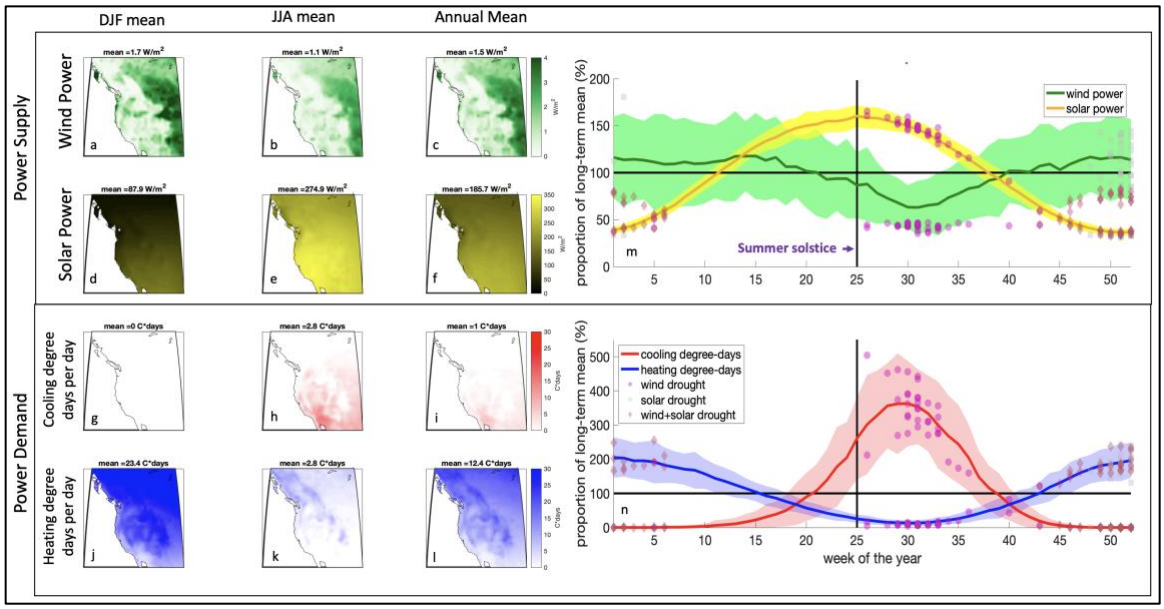

Fig. 1. Climatology of potential power supplied by wind and solar resources and potential power demanded via heating and cooling degree days. Left) spatial distribution of climatology for different portions of the year. The wind resource is converted to a realistic spatial density using a wind power curve and an assumption about turbine spacing while the solar resource is left as the raw incident solar radiation. This difference becomes inconsequential in subsequent analysis since both variable are normalized by their own mean. Right) temporal distribution of climatology with 1st percentile drought weeks highlighted.

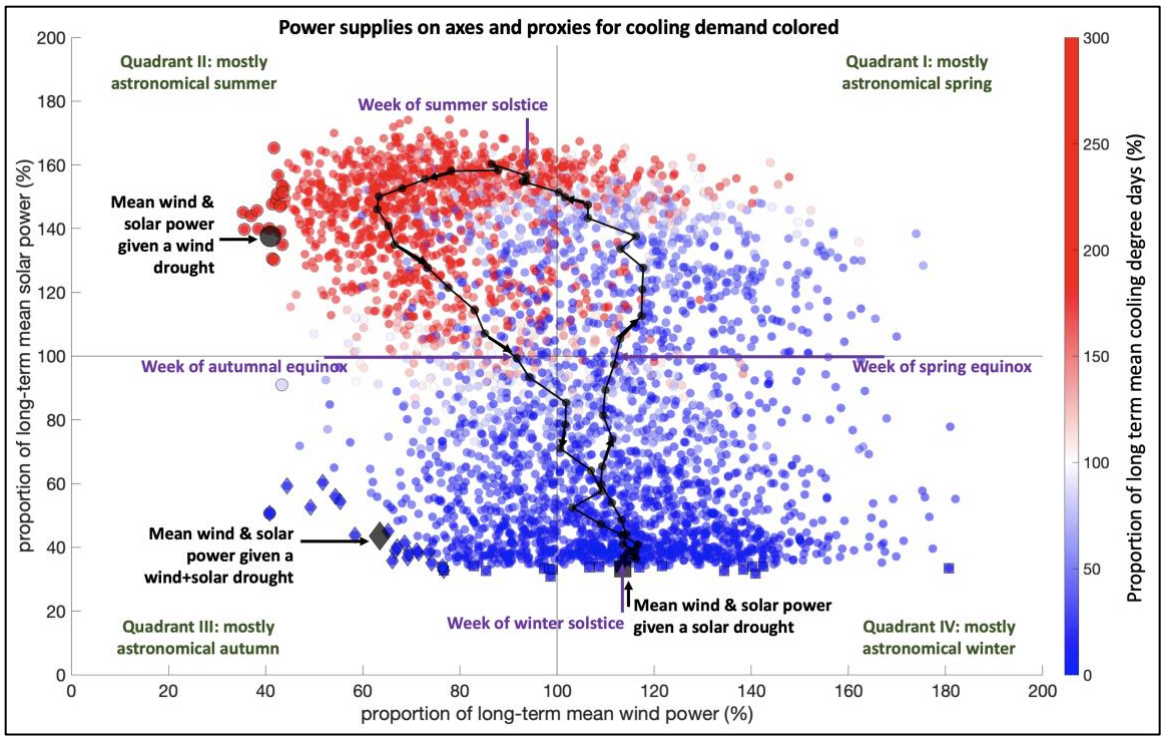

644

645 **Fig. 2.** All weekly values from 1950-2020 (average the western North America
646 domain, Fig. 1) for power supplied by wind and solar resources (x and y axes
647 respectively) and a proxy for power demanded via cooling degree days (color of dots).
648 The mean seasonal cycle in wind and solar power is shown by the black loop (52 black
649 dots for each week of the year). Drought weeks are indicated with black edge colors
650 with wind droughts represented as circles, solar droughts represented as squares and
651 compound wind and solar droughts represented as diamonds. An animation showing
652 the degree to which there is persistence in time can be seen here.

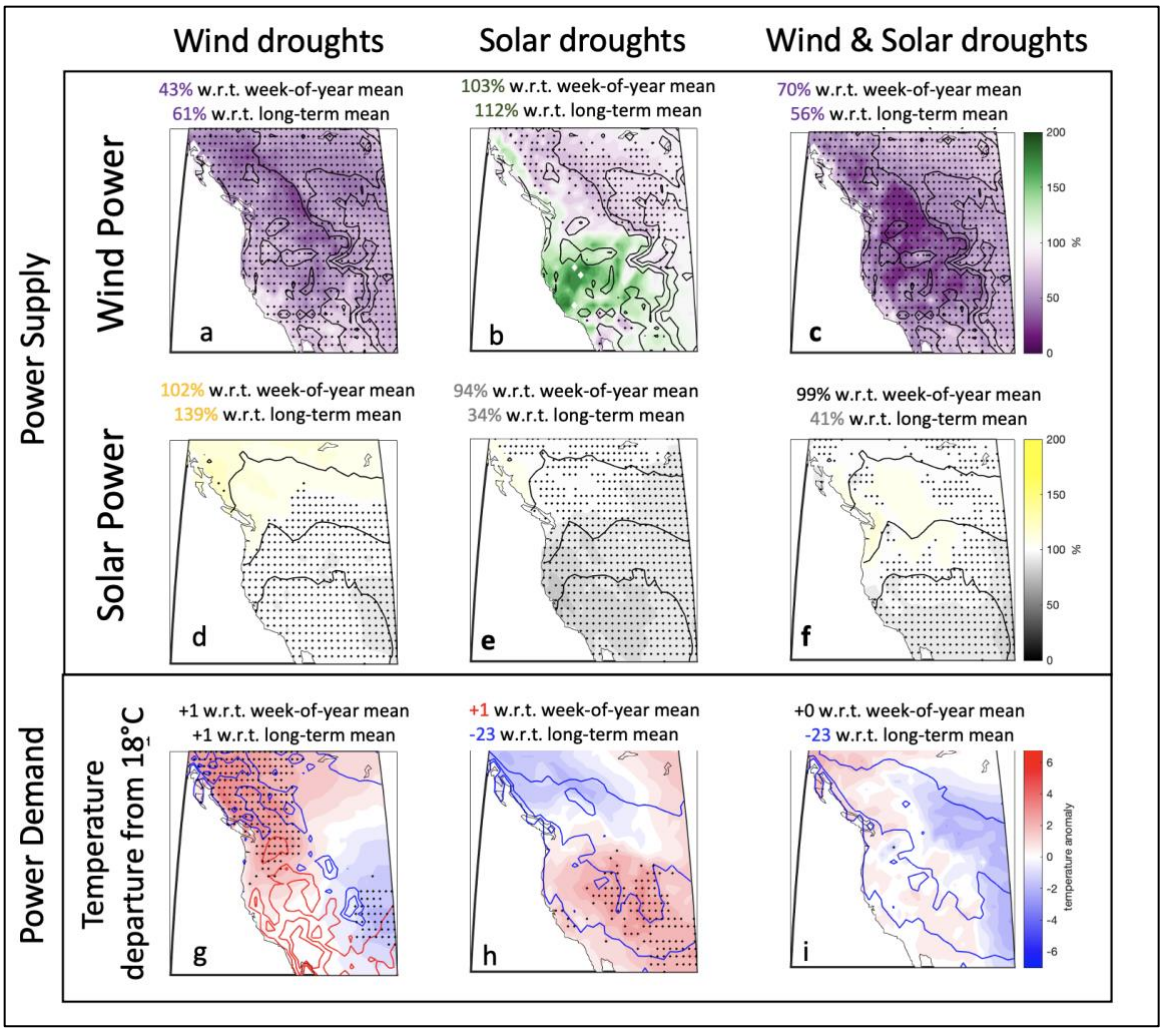

653

654 **Fig. 3.** Composites over the 37 weeks (out of 3692 weeks from 1950-2020) with the
655 lowest domain-average wind power (a,d,g), solar power (b,e,h) and combined wind
656 and solar power (c,f,i). The 37 most extreme weeks represent the ~1st percentile
657 across the dataset or equivalently, they represent extremes with approximately 2-
658 year return periods. The colored shading in each panel represents the mean anomaly
659 (either normalized or absolute) with respect to the typical value for that week of the
660 year and the stippling shows where at least 28 of the 37 weeks (>75%) showed
661 anomalies of the same sign. The mean anomalies with respect to the long-term
662 (annual) mean are displayed atop each panel. Climatological mean values from Fig. 1

663 are contoured in panels a-f while the absolute deviation from 18°C (65°F) are
664 contoured in g-i with positive values contoured red and negative values contoured
665 blue. Figs S5-S8 show plots for each individual drought event.

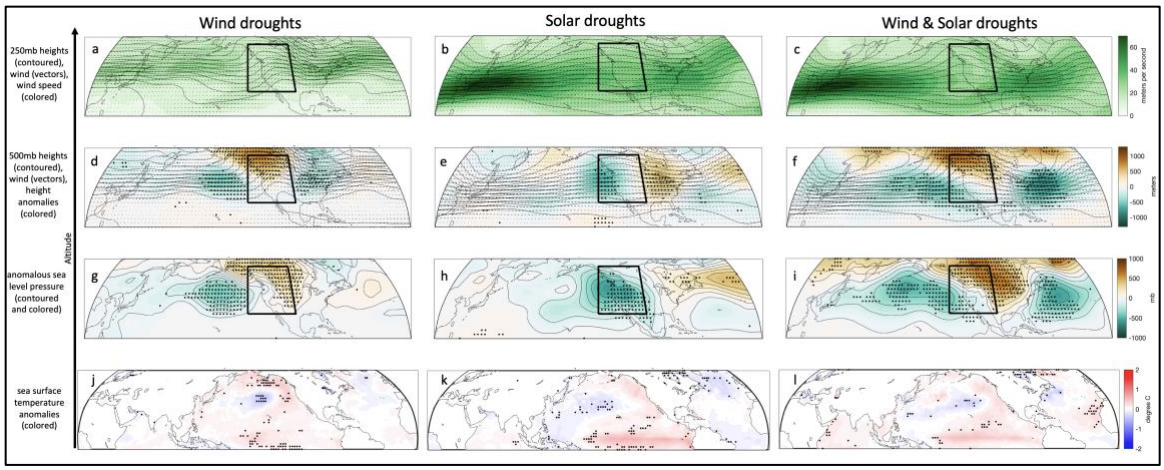

666

667 **Fig. 4.** Composites over the 37 weeks (out of 3692 weeks from 1950-2020) with the
668 lowest domain-average wind power (a,d,g,j), solar power (b,e,h,k) and combined
669 wind and solar power (c,f,I,l). The 37 most extreme weeks represent the ~1st
670 percentile across the dataset or equivalently, they represent extremes with
671 approximately 2-year return periods. The variables displayed are described on the
672 left. All anomalies are defined with respect to the typical value for that week of the
673 year and the stippling shows where at least 28 of the 37 weeks (>75%) showed
674 anomalies of the same sign. Figs S9-S11 show 500mb height plots for each individual
675 drought event and Figs S12-S14 show sea surface temperature anomaly plots for each
676 individual drought event.

677

678 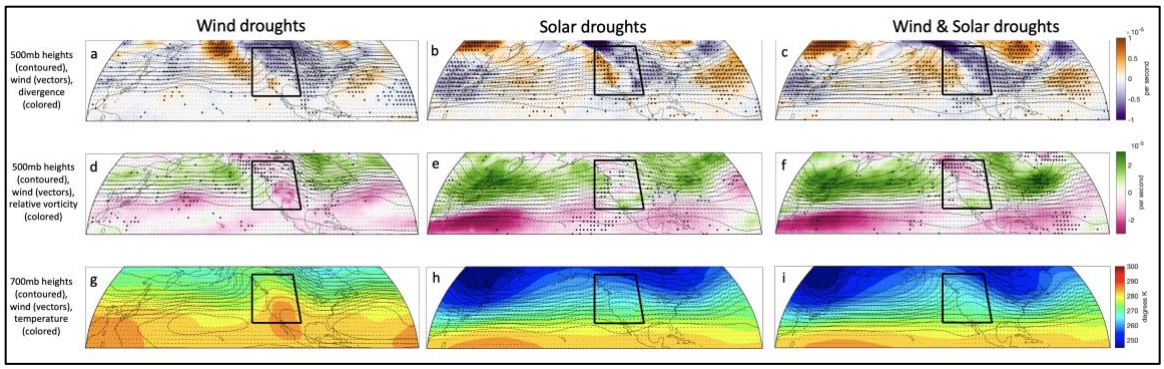

679 **Fig. 5.** Composites over the 37 weeks (out of 3692 weeks from 1950-2020) with the
680 lowest domain-average wind power (a,d,g), solar power (b,e,h) and combined wind
681 and solar power (c,f,i). The 37 most extreme weeks represent the ~1st percentile
682 across the dataset or equivalently, they represent extremes with approximately 2-
683 year return periods. The variables displayed are described on the left. The stippling
684 shows where at least 38 of the 37 weeks (>75%) showed values of the same sign.

685

Figures

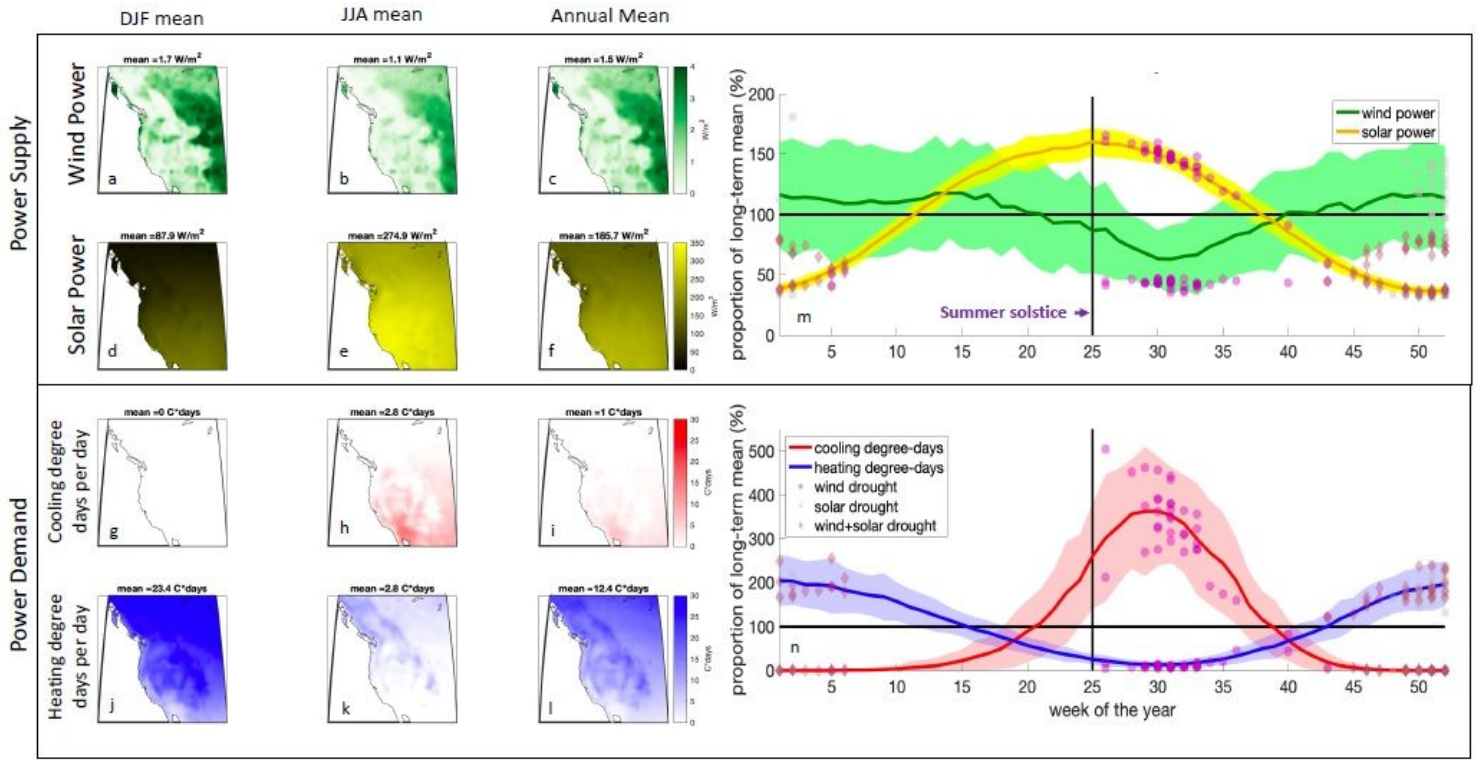

Figure 1

Climatology of potential power supplied by wind and solar resources and potential power demanded via heating and cooling degree days. Left) spatial distribution of climatology for different portions of the year. The wind resource is converted to a realistic spatial density using a wind power curve and an assumption about turbine spacing while the solar resource is left as the raw incident solar radiation. This difference becomes inconsequential in subsequent analysis since both variable are normalized by their own mean. Right) temporal distribution of climatology with 1st percentile drought weeks highlighted.

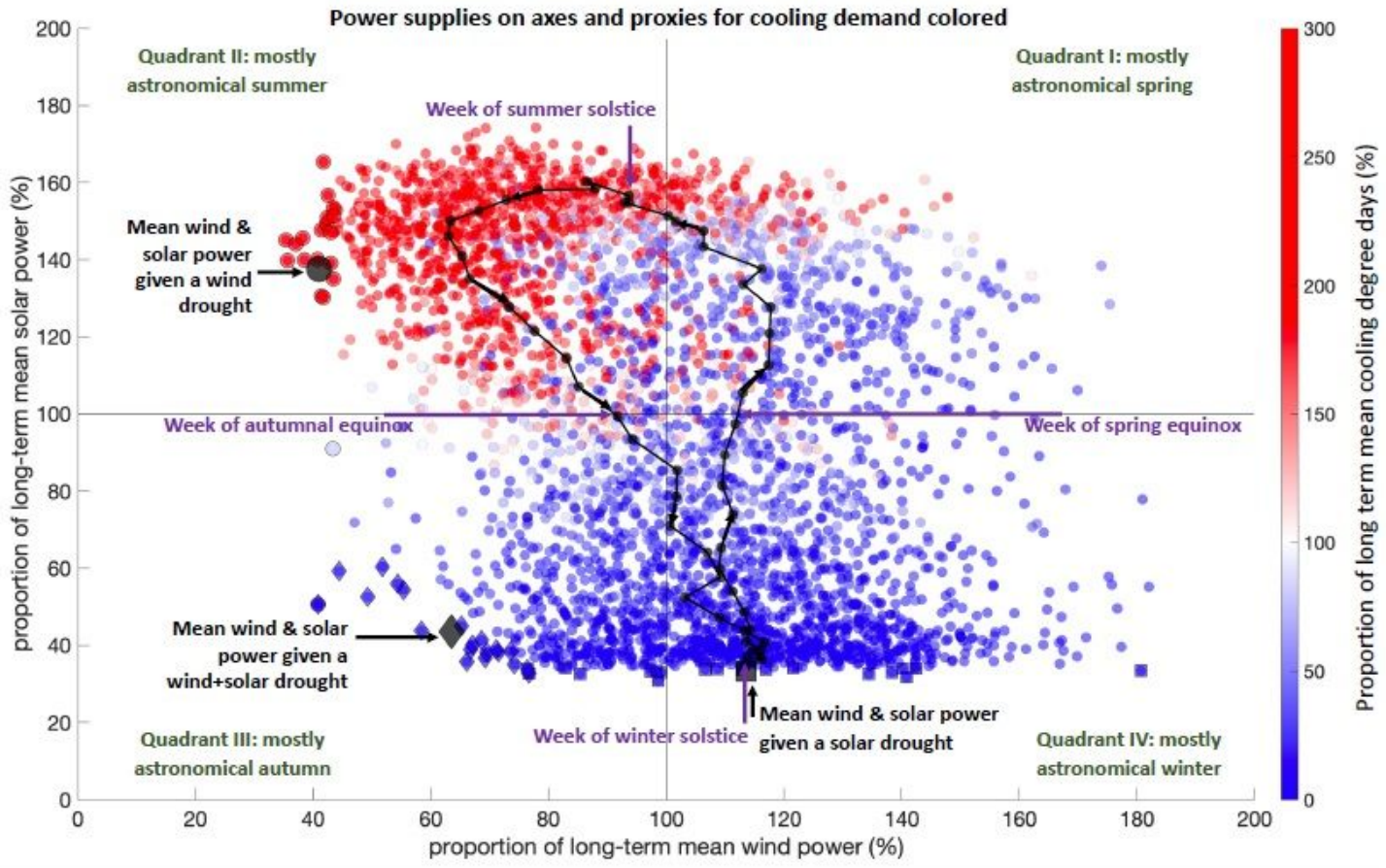

Figure 2

All weekly values from 1950-2020 (average the western North America domain, Fig. 1) for power supplied by wind and solar resources (x and y axes respectively) and a proxy for power demanded via cooling degree days (color of dots). The mean seasonal cycle in wind and solar power is shown by the black loop (52 black dots for each week of the year). Drought weeks are indicated with black edge colors with wind droughts represented as circles, solar droughts represented as squares and compound wind and solar droughts represented as diamonds. An animation showing the degree to which there is persistence in time can be seen here.

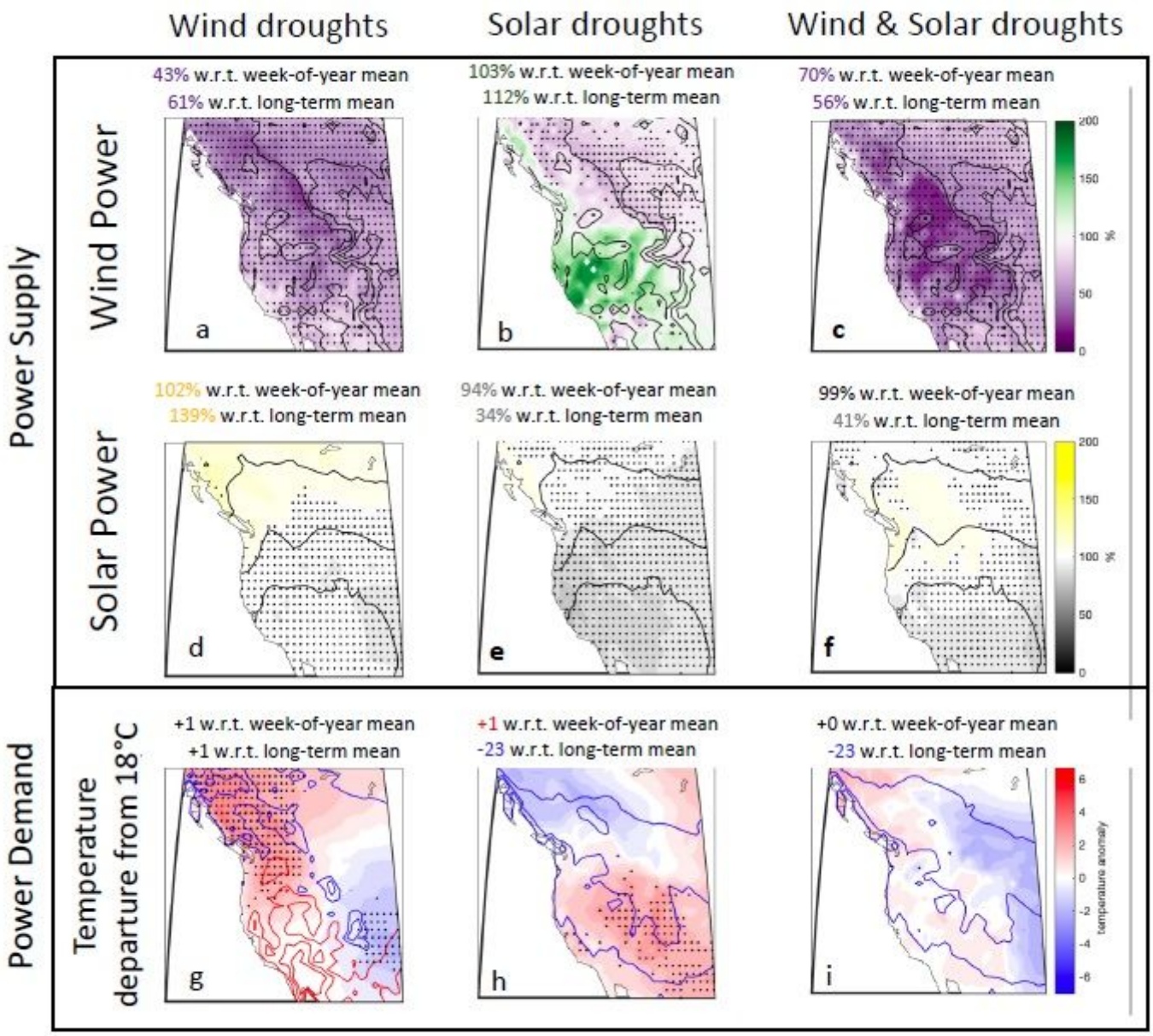

Figure 3

Composites over the 37 weeks (out of 3692 weeks from 1950-2020) with the lowest domain-average wind power (a,d,g), solar power (b,e,h) and combined wind and solar power (c,f,i). The 37 most extreme weeks represent the ~1st percentile across the dataset or equivalently, they represent extremes with approximately 2-year return periods. The colored shading in each panel represents the mean anomaly (either normalized or absolute) with respect to the typical value for that week of the year and the stippling shows where at least 28 of the 37 weeks (>75%) showed anomalies of the same sign. The mean anomalies with respect to the long-term (annual) mean are displayed atop each panel. Climatological mean values from Fig. 1 are contoured in panels a-f while the absolute deviation from 18°C (65°F) are contoured in g-i with positive values contoured red and negative values contoured blue. Figs S5-S8 show plots for each individual drought event.

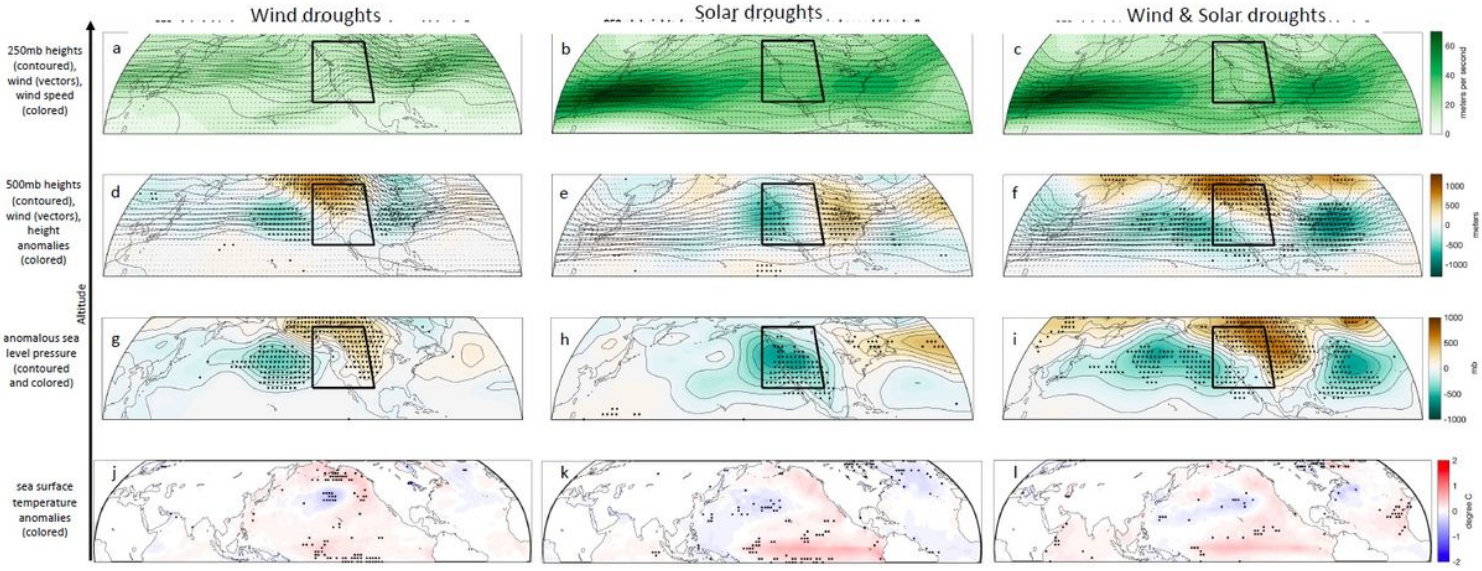

Figure 4

Composites over the 37 weeks (out of 3692 weeks from 1950-2020) with the lowest domain-average wind power (a,d,g,j), solar power (b,e,h,k) and combined wind and solar power (c,f,l,l). The 37 most extreme weeks represent the ~1st percentile across the dataset or equivalently, they represent extremes with approximately 2-year return periods. The variables displayed are described on the left. All anomalies are defined with respect to the typical value for that week of the year and the stippling shows where at least 28 of the 37 weeks (>75%) showed anomalies of the same sign. Figs S9-S11 show 500mb height plots for each individual drought event and Figs S12-S14 show sea surface temperature anomaly plots for each individual drought event.

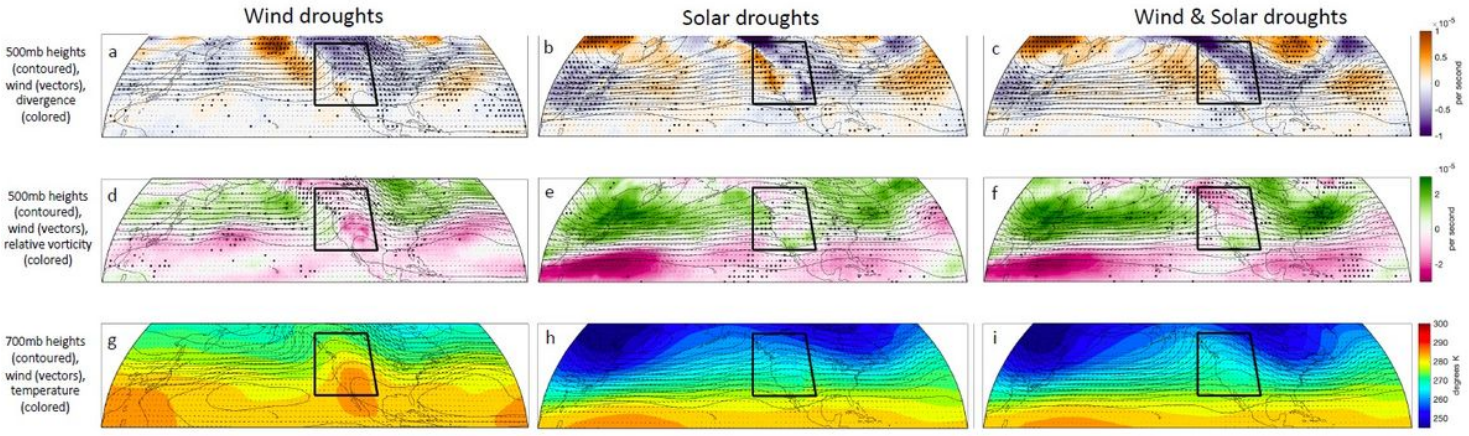

Figure 5

Composites over the 37 weeks (out of 3692 weeks from 1950-2020) with the lowest domain-average wind power (a,d,g), solar power (b,e,h) and combined wind and solar power (c,f,i). The 37 most extreme weeks represent the ~1st percentile across the dataset or equivalently, they represent extremes with

approximately 2-year return periods. The variables displayed are described on the left. The stippling shows where at least 38 of the 37 weeks (>75%) showed values of the same sign.

Supplementary Files

This is a list of supplementary files associated with this preprint. Click to download.

- BrownetalWSDroughtsSuppsubclimdyn.pdf